Biochimica et Biophysica Acta 1818 (2012) 467–473

Contents lists available at SciVerse ScienceDirect

Biochimica et Biophysica Acta

journal homepage: www.elsevier.com/locate/bbamem

Actin-dependent clustering of insulin receptors in membrane microdomains

Peter W. Winter [a], Alan K. Van Orden [b], Deborah A. Roess [a,c], B. George Barisas [a,b,*]

[a] Cell and Molecular Biology Program, Colorado State University, Fort Collins, CO 80523, USA
[b] Department of Chemistry, Colorado State University, Fort Collins, CO 80523, USA
[c] Department of Biomedical Sciences, Colorado State University, Fort Collins, CO 80523, USA

ARTICLE INFO

Article history:
Received 19 August 2011
Received in revised form 5 October 2011
Accepted 6 October 2011
Available online 15 October 2011

Keywords:
Insulin receptor
Photon counting histogram analysis
Single particle tracking
Polarization homo-transfer FRET
Membrane microdomain

ABSTRACT

Recent evidence suggests that, after binding insulin, insulin receptors (IR) interact with specialized, cholesterol-containing, membrane microdomains and components of the actin cytoskeleton. Using single particle tracking techniques, we examined how binding of insulin, depletion of membrane cholesterol and disruption of actin filaments affect the lateral diffusion of individual quantum dot-labeled native IR on live rat basophilic leukemia 2H3 cells. We also examined the effects of similar treatments on IR clustering and multivalent insulin binding on these cells using both photon counting histogram analysis and polarization-based fluorescence resonance energy homo-transfer imaging. Our analyses indicate that binding of insulin to IR on these cells is multivalent, involving at least two insulin molecules per IR as labeling concentrations approach 1 μM. Insulin binding also reduces lateral diffusion of IR and the size of membrane compartments accessed by IR. For IR that have not bound insulin, lateral diffusion of IR and the size of membrane compartments accessed by IR increase after disrupting actin filaments or depleting membrane cholesterol. However, clustering of insulin-occupied IR is reduced only by disrupting actin filaments or by fixing cells with paraformaldehyde prior to exposure to insulin, but not by depleting membrane cholesterol. Thus, it appears that, although restriction of IR lateral diffusion on these cells is sensitive to both actin filament dynamics and membrane cholesterol content, clustering of insulin-occupied IR primarily involves an actin-dependent mechanism.

1. Introduction

The insulin receptor (IR) is a well-characterized hetero-tetrameric $(\alpha\beta)_2$ transmembrane receptor, consisting of two extracellular α-subunits, containing multiple ligand-binding sites, and two largely intracellular β-subunits with both *auto*- and *trans*-tyrosine kinase activity [1–6]. Binding of ligand to IR α-subunits induces the phosphorylation of each β-subunit by the other, increasing the activity of both β-subunits and *in vitro* IR is known to exhibit complex allosteric ligand-binding properties [2–4].

Previous work by our group demonstrates that insulin treatment increases association of native IR and downstream substrates with detergent-resistant membrane microdomains on 2H3 rat basophilic leukemia (RBL-2H3) cells [7]. Similar results obtained by other investigators also indicate that, in adipocytes, IR preferentially associate with cholesterol-containing membrane microdomains [8–13] and that, in muscle cells, insulin treatment induces substantial reorganization of sub-surface actin filaments [14]. It has also been suggested that, in some cell types, components of the actin cytoskeleton anchor IR in specialized, cholesterol-containing, membrane microdomains such as caveolae [15]. However, the nature of these interactions and how they affect both lateral motions of IR and IR self-association, *i.e.* clustering, is not yet adequately characterized at the single-molecule level.

RBL-2H3 cells are well-characterized with respect to activation of the Type I Fcε receptor (FcεRI) by antigen crosslinking and, as observed for IR on other cell lines, activation of FcεRI on these cells results in increased association of FcεRI with specialized, cholesterol-containing, membrane microdomains [16–18]. Additionally, both restriction of individual FcεRI lateral motions and clustering of crosslinked FcεRI on these cells have also been shown to involve interactions with sub-surface actin filaments [16].

In the present work, we utilize single particle tracking (SPT) [18–22] to monitor the lateral motions of individual quantum dot-labeled IR diffusing on the surface of intact RBL-2H3 cells. We also utilize both photon counting histogram analysis (PCH) [23,24] and polarization-based fluorescence resonance energy homo-transfer (homoFRET) imaging [25–27] to investigate multivalent binding of ligand and clustering of ligand-occupied IR on these cells. We define a *cluster* as a group of receptors that diffuse together or otherwise lie within

Abbreviations: IR, insulin receptor; RBL-2H3, 2H3 rat basophilic leukemia; FcεRI, Type I Fcε receptor; SPT, single particle tracking; PCH, photon counting histogram analysis; homoFRET, polarization-based fluorescence resonance energy homo-transfer; FITC, fluorescein isothiocyanate; MβCD, methyl-β-cyclodextrin); BSA, bovine serum albumin; FITC-insulin, human recombinant insulin N-terminally tagged with FITC; R6G, rhodamine 6G; MEM, modified essential medium; FBS, fetal bovine serum; N, average number of particles detected; ε, photon counts per molecule; F, out-of-focus emission ratio; s, total intensity; r, fluorescence anisotropy; %E, FRET efficiencies; Δr, change in anisotropy.

* Corresponding author at: Department of Chemistry Campus Mail 1872, Colorado State University, Fort Collins, CO 80523, USA. Tel.: +1 970 491 6641; fax: +1 970 491 1801.
E-mail address: barisas@lamar.colostate.edu (B.G. Barisas).

0005-2736/$ – see front matter © 2011 Elsevier B.V. All rights reserved.
doi:10.1016/j.bbamem.2011.10.006

approximately 5 nm of one another, a distance at which substantial homoFRET between fluorescein isothiocyanate (FITC) labels occurs [28].

Our results indicate that at least two separate FITC-insulin molecules can bind to individual IR on the surface of live RBL-2H3 cells as labeling concentrations approach 1 μM, leading to increased restriction of individual IR lateral diffusion and a reduction in the size of membrane compartments accessed by IR. We also demonstrate that clustering of insulin-occupied IR on these cells is reduced by disrupting actin filaments or by fixing cells with paraformaldehyde prior to labeling. Finally, we show that, while depletion of cholesterol from cell membranes does not affect IR clustering, it does increase cell-surface IR lateral diffusion. Taken together, our results suggest that at least a portion of insulin-occupied IR are contained within nanometer-scale, cholesterol-containing, membrane microdomains but that clustering of insulin-occupied IR primarily depends on actin filament dynamics.

2. Materials and methods

2.1. Materials

RBL-2H3 cells were purchased from ATCC (Manassas, VA). Insulin, methyl-β-cyclodextrin (MβCD), paraformaldehyde, cytochalasin D and bovine serum albumin (BSA) were purchased from Sigma-Aldrich Inc. (St. Louis, MO). Anti-insulin receptor-β-biotin (C-19) IgG was purchased from Santa Cruz Biotech (Santa Cruz, CA). Human recombinant insulin N-terminally tagged with FITC (FITC-insulin) and Qdot605 streptavidin-conjugated quantum dots, were purchased from Invitrogen (Carlsbad, CA). Rhodamine 6G (R6G) was purchased from Allied Chemical (Vadodara, Gujarat, India). Modified essential medium (MEM) was purchased from Cellgro (Manassas, VA). Fetal bovine serum (FBS) and Fungizone were purchased from Gemini (Sacramento, CA). Sodium fluorescein was purchased from Merck (Whitehouse Station, NJ).

2.2. Sample preparation

For SPT, PCH and homoFRET experiments, RBL-2H3 cells were seeded onto sterile #1.5 glass bottom culture dishes, grown to approximately 50% confluence and, unless otherwise indicated, incubated in medium without FBS for a minimum of 12 h before use to remove a source of exogenous insulin and other hormones. In some experiments cells were treated with either 40 μg/mL cytochalasin D or 10 mM MβCD or with both cytochalasin D and MβCD for 1 h at 37 °C before labeling.

2.3. PCH of FITC-insulin labeled insulin receptors

In FITC-insulin equilibrium binding experiments, cells were incubated in 0.01 nM–1 μM FITC-insulin for 30 min, followed by 4 washes. In competition binding experiments between FITC-insulin and insulin, cells were simultaneously incubated in buffer solutions containing 50 nM FITC-insulin and increasing amounts of insulin for 30 min then washed 4 times. To measure FITC-insulin dissociation, cells were labeled with 10 nM FITC-insulin for 30 min, washed 4 times and then examined at the times indicated. To investigate the effects of aqueous insulin on FITC-insulin dissociation, cells were labeled with 250 nM FITC-insulin for 30 min, washed 3 times for 30 sec in 1 mL of buffer and then incubated in 0.025 nM–25 μM insulin for 30 min and washed 3 times.

PCH experiments were performed using a modified Nikon TE1000 inverted microscope equipped with a 100×, 1.25 NA, oil-immersion objective, an Omnichrome Melles–Griot multi-line air-cooled argon ion laser, two PerkinElmer single photon counting modules (SPCM-AQR-14), an ALV-6010 digital hardware correlator and a Becker and Hickl GmbH PMS-400 multichannel correlator as previously described [29]. Based on FCS measurements of aqueous R6G diffusion, the $1/e^2$ radius of the laser excitation beam at the sample in our system was determined to be 241 nm. In live cell studies, the laser was focused on the apical cell membrane to maximize detector count rates and minimize diffusional correlation times as described by Ries and Schwille [30]. Samples were illuminated for approximately 10 s before collection of data to irreversibly photobleach immobile particles [31]. Data were then collected for 30 s during which time the average fluorescence from the sample was relatively uniform as indicated by the avalanche photodiode signal readouts. For PCH, detected photons were accumulated into successive 1 μs counting channels and then rebinned into 9 μs channels to improve signal-to-noise ratios. Accumulated photon counts were then simultaneously subjected to autocorrelation, pseudo-autocorrelation and PCH. Weighted least-squares fitting was used to obtain estimates of the average number of particles (N) in the interrogation volume, the detected photon counts per molecule (ε) per sampling time, also known as the molecular brightness, and the out-of-focus emission ratio (F) as previously described [24,32,33]. Each PCH value presented, except those in Table 3, represents the result of measurements on 8–10 individual RBL-2H3 cells. Each PCH value presented in Table 3 represents a single measurement from an individual cell.

2.4. Single particle tracking of individual insulin receptors

Fluorescent quantum dots were used to track the lateral motions of individual IR on the surface of live RBL-2H3 cells. Briefly, viable RBL-2H3 cells were labeled using a slight modification of a protocol that minimizes receptor crosslinking [19]. Cells were first labeled with anti-IR-β-biotin IgG at 0.1 μg/mL for 30–40 min, washed 3 times for 1 min in 1 mL of buffer, labeled with 100 pM Qdot605 streptavidin-conjugated quantum dots for 10 min and then washed 6 times for 1 min in 1 mL of buffer before imaging. Wide-field fluorescence images were then collected from the apical surface of live cells using a Zeiss Axiovert 200 M microscope equipped with a 63× 1.2 NA apochromatic water-immersion objective and custom filter sets (Chroma Technology; Bellow Falls, VT). Images were collected every 33 ms for up to 3 min at a total magnification of 315× with an Andor Ixon EM+ camera resulting in a final pixel size of approximately 50 nm. This was achieved using a Zeiss 2.5× Optovar and a 2× C-mount magnifying lens placed in front of the camera. Image acquisition and determination of individual particle locations were performed with MetaMorph 7.1.6 (Molecular Devices; Sunnyvale, CA). Macroscopic lateral diffusion rates and compartment diagonals were determined using custom analysis programs. Blinking of individual IR-bound quantum dot particles, while apparent, did not prevent tracking over long periods of time. The trajectories of individual particles were segmented into compartments by calculation of statistical variance in particle position over time [18] producing variance plots that exhibited peaks at inter-compartment boundaries. These results were analyzed to yield the compartment sizes and time of residence in these compartments for each particle. Effective macroscopic diffusion was calculated as the square of the compartment diagonal divided by four times the residence time in the compartment as previously described [34]. SPT values shown each reflect measurements of 30–100 total particles on 10–20 individual RBL-2H3 cells.

2.5. HomoFRET imaging of FITC-insulin labeled insulin receptors

We used homoFRET methods similar to those previously described [35] to examine multivalent ligand binding and clustering of ligand-occupied IR. Data were acquired on individual, FITC-insulin labeled RBL-2H3 cells using an Olympus IX-71 microscope equipped with a FV300 confocal scanning unit, a 60×, 1.2NA apochromatic water-immersion objective, and a polarizing beam splitter to allow simultaneous collection of parallel and perpendicular fluorescence. FITC-insulin was excited with the 488 nm line of an argon ion laser and appropriate barrier and dichroic filters were selected for fluorescence

emission. Individual cells emitting ring-like fluorescence from FITC-insulin labeling at the plasma membrane were selected for imaging. Sequences of 30 cell images where then obtained as probe molecules were photobleached to approximately 10% of their initial average intensity. Image analysis was performed using custom data analysis programs. Total intensity (s) and fluorescence anisotropy (r) in the annular image region corresponding to the cell plasma membrane were calculated as $s = I_{\parallel} + 2I\perp$ and $r = (I_{\parallel} - I\perp)/s$, where $I_{\parallel}$ and $I\perp$ are fluorescence emission polarized parallel and perpendicular, respectively, to the polarization of excitation light [25,36]. FRET efficiencies (%E) were estimated from average initial and final r values using the following formula: $\%E = (1 - r_{initial}/r_{final}) \times 100\%$ [37]. The variance in change (Δr) in anisotropy values between individual cells was less than the variance of corresponding initial and final r values. This is due to irreproducibility in optical positioning that contributes to uncertainty in both $r_{initial}$ and r_{final}, but not in the difference Δr in these quantities. HomoFRET values shown each represent the result of measurements on 25–30 individual RBL-2H3 cells.

2.6. Presentation of results

All values presented except those in Table 4 are the mean ± SD. Values presented in Table 4 are the mean ± SEM.

3. Results

3.1. PCH of aqueous fluorophores

PCH provides a probability distribution for the number of detected photons observed during a specified counting interval and depends on the average photodetection rate for each fluorescing species in the system [23,24,33]. For each fluorescing species present, PCH is able to determine both molecular brightness ε and the effective number of particles residing in the interrogation volume *N*[38–41]. We utilized PCH to compare the molecular brightness of aqueous fluorescein and FITC-insulin (Fig. 1). Our results demonstrate that the molecular brightness of both fluorescein and FITC-insulin were similar at 0.13 ± 0.01 kHz and that, in solution, the molecular brightness of FITC-insulin was constant over a concentration range of 1–100 nM (data not shown).

3.2. PCH of FITC-insulin bound to insulin receptors on live-cells

We next utilized PCH to examine the molecular brightness of IR-bound FITC-insulin molecules on viable RBL-2H3 cells. The increased molecular brightness of FITC-insulin molecules when bound to IR diffusing on the surface of these cells relative to when diffusing in solution suggests either that IR separately bind at least two insulin molecules as labeling concentrations approach 1 μM or that insulin binding induces substantial clustering of cell-surface IR. Equilibrium binding of 10 pM–1 μM FITC-insulin shows that as the number of particles detected *N* increased, the molecular brightness of these particles also increased from 0.14 ± 0.01 kHz to 0.31 ± 0.07 kHz (Fig. 1 and Table 1). Treatment of cells with cytochalasin D or MβCD before labeling with 1 μM FITC-insulin slightly lowered the molecular brightness of detected particles to 0.27 ± 0.06 kHz and 0.29 ± 0.04 kHz, respectively, (Table 1) suggesting that the increase in molecular brightness of FITC-insulin when bound to IR may, in addition to multivalent insulin binding, also reflect clustering of a portion of cell-surface IR via an actin-mediated or cholesterol-dependent mechanism.

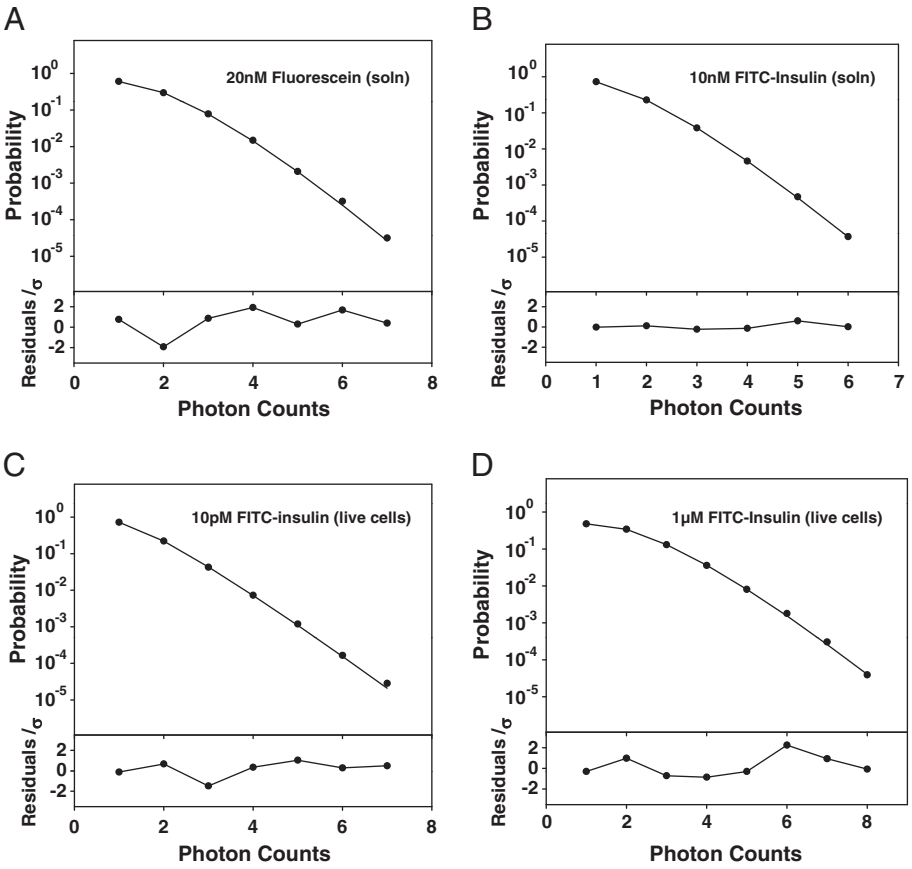

Fig. 1. Representative PCH of fluorescein-derived fluorescent probes in solution and on viable RBL-2H3 cells. A) 20 nM fluorescein (solution); ε 0.13, *N* 18.1, *F* 0.7, reduced χ^2 2.3, B) 10 nM FITC-insulin (solution); ε 0.11, *N* 12.7, *F* 0.7, reduced χ^2 0.15, C) 10 pM FITC-insulin (live-cells); ε 0.13, *N* 3.2, *F* 0.7, reduced χ^2 1.1, D) 1 μM FITC-insulin (live-cells); ε 0.3, *N* 26.7, *F* 0.7, reduced χ^2 1.2.

Table 1
PCH of equilibrium binding of FITC-insulin to RBL-2H3 cells.

FITC-insulin (nM)	Treatment	*N* (particles)	ε (kHz)[a]
0.01	None	3.4 ± 1.0	0.14 ± 0.01
0.1	None	4.8 ± 1.7	0.15 ± 0.01
1.0	None	7.9 ± 3.2	0.17 ± 0.02
10	None	8.9 ± 3.2	0.20 ± 0.04
25	None	15.3 ± 3.1	0.24 ± 0.03
250	None	19.8 ± 3.2	0.23 ± 0.02
1000	None	23.5 ± 4.4	0.31 ± 0.07
1000	MβCD	20.0 ± 9.0	0.29 ± 0.04
1000	Cytochalasin D	19.0 ± 9.2	0.27 ± 0.06

[a] Estimates of molecular brightness ε were obtained using a detector bin time of 9 μs and out-of-focus emission factor *F* values from 0.3 to 0.9.

Similar information on the concentration dependence of insulin binding was obtained by competitive labeling at a fixed FITC-insulin concentration of 50 nM together with 25 pM–25 μM concentrations of unlabeled insulin. These experiments indicate that the molecular brightness of cell-bound FITC-insulin decreased from 0.25 ± 0.04 kHz to 0.17 ± 0.02 kHz as *N* decreased (Table 2).

PCH monitoring the dissociation of FITC-insulin from cells over a 2 h period provided an alternative method for evaluating the change in molecular brightness with respect to the level of ligand-IR occupancy and indicates that the molecular brightness of detected particles on cells labeled with 10 nM FITC-insulin decreased from approximately 0.18 kHz to 0.14 kHz as *N* decreased from approximately 9 to 2 (Table 3). Moreover, the molecular brightness of detected particles also decreased from 0.26 ± 0.05 kHz to 0.19 ± 0.06 kHz in separate experiments where cells were labeled with 250 nM FITC-insulin for 30 min and then incubated in either 50 pM or 50 μM insulin, respectively, for 30 min before observation. Combined, these results indicate that changes in the number of detected particles *N* are mirrored by changes in molecular brightness ε which is consistent with multivalent binding of insulin to IR and/or clustering of insulin-occupied IR.

3.3. Lateral diffusion of individual cell-surface insulin receptors

Examination of PCH results (Table 1) indicate that treatment with 50 nM or greater concentrations of insulin results in the occupancy of at least 75% of insulin binding sites on viable RBL-2H3 cells. With this in mind, we examined the lateral diffusion of IR on the surface of live RBL-2H3 cells before and after treatment with both 50 nM and 250 nM insulin (Fig. 2 and Table 4). When anti-IRβ-biotin IgG and streptavidin-conjugated quantum dots were used to track the movement of individual IR on serum-starved cells, the average macroscopic lateral diffusion coefficient was approximately 1×10^{-10} cm^2 s^{-1}. After treatment with insulin this was reduced to approximately 3×10^{-11} cm^2 s^{-1} (Fig. 2 and Table 4). The average size of compartments accessed by IR was also reduced from approximately 475 nm in serum-starved cells to approximately 250 nm after insulin treatment (Fig. 2 and Table 4). Treatment of serum-starved cells for 1 h with either 40 μg/mL cytochalasin D or 10 mM MβCD increased IR lateral diffusion to approximately 2×10^{-9} cm^2 s^{-1} and 1×10^{-9} cm^2 s^{-1}, respectively (Table 4) and increased the size of membrane compartments accessed by IR to approximately 1 μm and 600 nm, respectively. The increases in IR lateral diffusion and compartment size caused by disrupting actin filaments were almost two-fold greater than those produced by depleting membrane cholesterol content. This suggests that restriction of individual cell-surface IR lateral diffusion is regulated differentially by cholesterol-containing membrane structures and sub-surface cytoskeletal actin filaments.

Table 2
PCH of competition binding between 50 nM FITC-insulin and insulin on RBL-2H3 cells.

Insulin (nM)	*N* (particles)	ε (kHz)[a]
0.025	12.6 ± 3.1	0.25 ± 0.04
0.25	10.1 ± 4.0	0.24 ± 0.03
2.5	8.3 ± 3.6	0.24 ± 0.04
25	8.4 ± 4.3	0.22 ± 0.02
250	4.0 ± 1.3	0.21 ± 0.02
2500	3.9 ± 1.3	0.20 ± 0.02
25,000	2.4 ± 0.5	0.17 ± 0.02

[a] Estimates of molecular brightness ε were obtained using a detector bin time of 9 μs and out-of-focus emission factor *F* values from 0.3 to 0.9.

Table 3
PCH of 10 nM FITC-insulin dissociating from IR on the surface of RBL-2H3 cells.

Dissociation time (min)	*N* (particles)	ε (kHz)[a]
0	8.9	0.18
9	6.5	0.19
18	7.6	0.17
27	3.4	0.16
36	6.6	0.16
45	2.2	0.15
54	2.9	0.15
63	3.0	0.15
72	4.6	0.14
81	2.6	0.15
90	2.6	0.13
99	1.7	0.14
108	1.3	0.13
117	2.2	0.14

[a] Estimates of molecular brightness ε were obtained using a detector bin time of 9 μs and out-of-focus emission factor *F* values from 0.3 to 0.9.

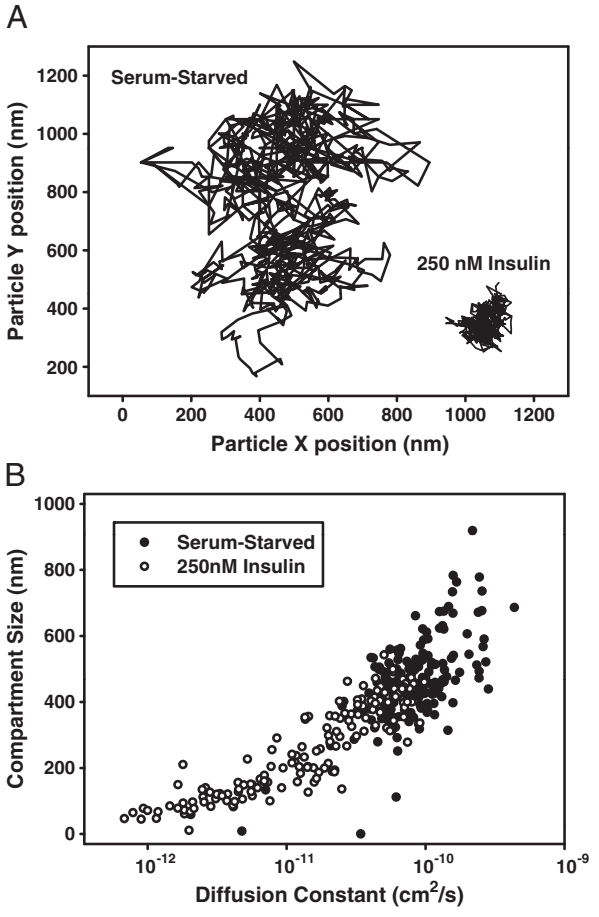

Fig. 2. A) Representative trajectories of quantum dot-labeled IR from a serum-starved RBL-2H3 cell and a cell treated with 250 nM insulin. B) Average lateral diffusion vs. average compartment diagonal for individual quantum dot labeled IR on serum starved cells or cells treated with 250 nM insulin.

Table 4
SPT measurements of quantum dot-labeled IR on live RBL-2H3 cells before and after treatment with insulin, cytochalasin D or MβCD.

Treatment	Macroscopic diffusion rate (10^{-10}cm^{2}s^{-1})	Compartment diagonal (nm)
Untreated	1.00 ± 0.05	472 ± 9
50 nM insulin	0.34 ± 0.07[a]	239 ± 22[a]
250 nM insulin	0.27 ± 0.02[a]	266 ± 11[a]
40 μg/mL cytochalasin D	17.1 ± 2.5[a]	984 ± 94[a]
10 mM MβCD	11.2 ± 1.4[a]	599 ± 46[a]

[a] Values are significantly different from respective values measured on untreated cells as judged by Student's *t*-test ($p<0.01$).

3.4. HomoFRET imaging of FITC-insulin-occupied cell-surface insulin receptors

We next examined multivalent binding of insulin and insulin-induced clustering of IR using homoFRET imaging. Like PCH, homoFRET is useful for monitoring the clustering of biological molecules on the macromolecular scale (~10 nm) [25–27], and also yields information on multivalent binding of ligand [35]. HomoFRET between neighboring, fluorescent molecules is easily observed by monitoring changes in the anisotropy r of fluorescence emission as probe molecules are progressively photobleached [27,35]. Analysis of IR clustering on live, serum-starved, but otherwise untreated, RBL-2H3 cells labeled with 10 nM FITC-insulin indicates that the initial anisotropy of receptor bound FITC-insulin is 0.18 ± 0.02 and increases 0.02 ± 0.02 as probe molecules are bleached to approximately 10% of their original intensity (Table 5). Using the method originally developed by Yao and Major [37], we calculate that the efficiency %E of homoFRET transfer between FITC-insulin molecules bound to these cells is 14%. On similar serum-starved, but otherwise untreated, RBL-2H3 cells, IR labeled with 1 μM FITC-insulin exhibit an initial anisotropy of 0.13 ± 0.02 which, upon bleaching, increases by 0.06 ± 0.01, implying a %E of 32% (Fig. 3, Table 5). This increase in %E observed for the higher FITC-insulin labeling concentration suggests the onset of lower-affinity multivalent ligand binding and/or insulin-induced IR clustering.

Extraction of membrane cholesterol from cells using MβCD decreased the initial anisotropy of IR labeled with 1 μM FITC-insulin to 0.10 ± 0.02 and decreased the total change in anisotropy as probe molecules were bleached to 0.05 ± 0.01. However, the %E of FITC-insulin labeled IR on such cells was nearly identical to the %E of cells that were untreated before labeling with 1 μM FITC-insulin (Table 5). Disruption of actin filaments using cytochalasin D decreased the total change in anisotropy as probe molecules were bleached to 0.04 ± 0.01 and decreased the %E of IR labeled with 1 μM FITC-insulin to 21%, but had no effect on the initial anisotropy of these molecules (Table 5). Simultaneous treatment of cells with MβCD and cytochalasin D reduced both the final anisotropy of IR labeled with 1 μM FITC-insulin to 0.15 ± 0.02 and reduced %E to 20%. Finally, homoFRET analysis of cells fixed in 4% paraformaldehyde for 40 min at 37 °C before labeling IR with 1 μM FITC-insulin shows that, while the initial and final anisotropy of IR bound FITC-insulin slightly increased, the total change in anisotropy during bleaching of probe molecules decreased to 0.04 ± 0.01 resulting in a %E of 25% (Table 5). Fixing cells with paraformaldehyde before labeling presumably reduces changes in cell-surface IR distribution that would otherwise result from exposure to FITC-insulin [42]. This suggests that, in addition to homoFRET resulting from multivalent binding of FITC-insulin to IR, at least a portion of the homoFRET between IR-bound FITC-insulin molecules on live, otherwise untreated, cells is due to insulin-induced IR clustering not seen in cells fixed with paraformaldehyde or treated with cytochalasin D before labeling.

4. Discussion

How hierarchical organization of the plasma membrane affects both lateral motions and spatial distribution of transmembrane protein receptors is of considerable interest [11,13–15,43,44]. Therefore, we examined how the interaction of a transmembrane receptor such as IR with cholesterol-containing membrane structures and actin filament-delineated membrane compartments affected both clustering and lateral motions of IR using a variety of fluorescence-based biophysical techniques.

A growing body of evidence suggests that several types of membrane structures and microdomains serve as platforms for IR signaling [11–13,45–49] and that components of the actin cytoskeleton anchor IR in microdomains such as caveolae [15]. However, the effects of both membrane cholesterol depletion and disruption of actin filament dynamics on clustering of ligand-occupied IR and the restriction of individual IR lateral motions have not been adequately described at the single molecule level.

PCH of FITC-insulin binding to native IR on live RBL-2H3 cells suggests that IR ligand-binding is multivalent and likely involves at least two FITC-insulin molecules as labeling concentrations approach 1 μM. This is evident from comparison of the molecular brightness of FITC-insulin in solution and when bound to IR on the surface of RBL-2H3 cells. Increases in the molecular brightness of IR-bound FITC-insulin molecules as labeling concentration increase suggest that insulin binds IR multivalently at these higher concentrations. However, PCH alone cannot eliminate the possibility that the shift in molecular brightness observed as FITC-insulin molecules bind to live RBL-2H3 cells is the result of ligand-induced physical crosslinking of multiple IR; however, there is significant evidence, both *in vitro* and in live cells, indicating this does not occur [1–4].

Single particle tracking studies of IR lateral diffusion on live cells showed that, before insulin treatment, individual IR exhibit pseudo-random lateral diffusion within relatively large membrane microdomains. After exposure to insulin, individual IR largely become confined within 100 nm-400 nm scale microdomains and exhibit significantly reduced lateral diffusion. Although SPT studies cannot conclusively determine the mechanisms behind this ligand-induced restriction of IR lateral motion, they suggest that both actin filament dynamics and membrane cholesterol content regulate IR lateral motions on RBL-2H3 cells. These results also seem to support previous investigations which indicate that the plasma membrane contains hierarchically-organized lipid and protein-delineated compartments [20,43,50,51].

HomoFRET measurements on cells labeled with 10 nM FITC-insulin, under which conditions presumably largely high-affinity sites are occupied, suggest a degree of clustering is already present under this receptor ligation state. Comparison of homoFRET results for IR labeled with

Table 5
HomoFRET measurements of FITC-insulin labeled IR on RBL-2H3 cells.

Treatment	[FITC-insulin] (nM)	Initial r	Final r	Δr	%E
Serum starved	10	0.18 ± 0.02[a]	0.21 ± 0.03	0.02 ± 0.02[a]	14
Serum starved	1000	0.13 ± 0.02	0.19 ± 0.02	0.06 ± 0.01	32
4% paraformaldehyde	1000	0.15 ± 0.02[a]	0.20 ± 0.02	0.04 ± 0.01[a]	25
40 μg/mL cytochalasin D	1000	0.15 ± 0.02[a]	0.19 ± 0.02	0.04 ± 0.01[a]	21
10 mg/mL MβCD	1000	0.10 ± 0.02[a]	0.15 ± 0.02[a]	0.05 ± 0.01[a]	33
MβCD and cytochalasin D	1000	0.12 ± 0.01	0.15 ± 0.02[a]	0.03 ± 0.01[a]	20

[a] Values significantly different from respective values measured on serum starved cells labeled with 1000 nM FITC-insulin as judged by Student's *t*-test ($p<0.01$).

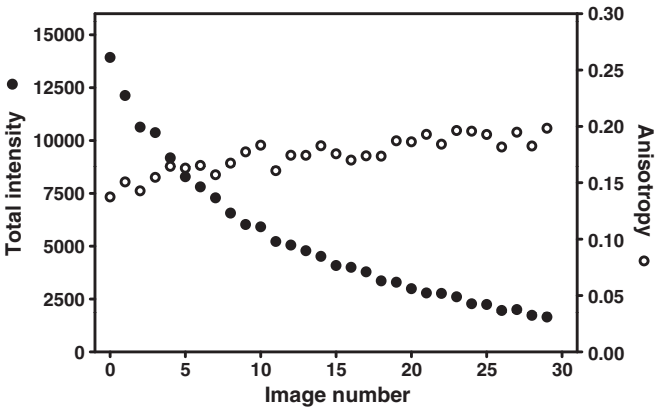

Fig. 3. Representative graph illustrating the change in anisotropy and total fluorescence intensity of IR-bound FITC-insulin molecules during the acquisition of 30 sequential images on a RBL-2H3 cell that was serum starved, but otherwise untreated, before labeling with 1 μM FITC-insulin.

10 nM and 1 μM FITC-insulin, respectively, suggests that high insulin concentrations increase the proximity of IR-bound FITC-insulin molecules. However, cell fixation with paraformaldehyde prior to exposure to 1 μM FITC-insulin reduced homoFRET, suggesting that the increases in homoFRET observed at higher labeling concentrations are at least in part due to IR clustering. The reduction in homoFRET efficiency relative to untreated cells when samples were treated with cytochalasin D, but not when treated with MβCD before labeling, suggests that this increased proximity arises due to insulin-induced clustering of IR via an actin-dependent mechanism that is not directly tied to membrane cholesterol content. This is interesting in light of prior evidence indicating that binding of ligand causes preferential association of IR with a variety of cholesterol-containing membrane microdomains [8–10] and that clustering of cell-surface EGFR increases after depleting membrane cholesterol [38]. It should be noted that, in the present study, MβCD depletion of membrane cholesterol, while not affecting IR clustering, did reduce the apparent initial anisotropy of FITC-insulin labeled IR. This is perhaps the result of increased nanosecond orientational fluctuations of the FITC-insulin labeled IR within the cell membrane.

Taken together, our results indicate that native IR on live RBL-2H3 cells bind at least two FITC-insulin molecules at labeling concentrations approaching 1 μM and that binding of ligand to these cells results in significant restriction of individual IR lateral motions. Our results also indicate that clustering of ligand-occupied IR on these cells involves an actin-dependent mechanism and does not depend on retention of IR within cholesterol-containing membrane microdomains.

Acknowledgements

We would like to thank Dr. Jaemyong Jung for writing PCH data acquisition and analysis software. We would also like to thank Dr. Jeffrey T. McPhee and Mr. Jonathan Gerding for assistance with acquisition of PCH data. This work was supported in part by grants CHE0628260 and MCB1024668 from the National Science Foundation.

References

[1] L. Chang, S.-H. Chiang, A.R. Saltiel, Insulin signaling and the regulation of glucose transport, Mol. Med. 10 (2004) 65–71.
[2] P. De Meyts, J. Whittaker, Structural biology of insulin and IGF1 receptors: implications for drug design, Nat. Rev. Drug Discov. 1 (2002).
[3] L. Gauguin, B. Klaproth, W. Sajid, A.S. Andersen, K.A. McNeil, B.E. Forbes, P. De Meyts, Structural basis for the lower affinity of the insulin-like growth factors for the insulin receptor, J. Biol. Chem. 283 (2008) 2604–2613.
[4] V.V. Kiselyov, S. Versteyhe, L. Gauguin, P. De Meyts, Harmonic oscillator model of the insulin and IGF1 receptors' allosteric binding and activation, Mol. Syst. Biol. 5 (2009) 243.
[5] R.T. Watson, M. Kanzaki, J.E. Pessin, Regulated membrane trafficking of the insulin-responsive glucose transporter 4 in adipocytes, Endocr. Rev. 25 (2004) 177–204.
[6] A. Saltiel, J. Pessin, Insulin signaling in microdomains of the plasma membrane, Traffic 4 (2003) 711–716.
[7] D.A. Roess, S.M.L. Smith, P. Winter, J. Zhou, P. Dou, B. Baruah, A.M. Trujillo, N.E. Levinger, X. Yang, B.G. Barisas, D.C. Crans, Effects of vanadium-containing compounds on membrane lipids and on microdomains used in receptor-mediated signaling, Chem. Biodivers. 5 (2008) 1558–1570.
[8] S. Parpal, M. Karlsson, H. Thorn, P. Stralfors, Cholesterol depletion disrupts caveolae and insulin receptor signaling for metabolic control via insulin receptor substrate-1, but not for mitogen-activated protein kinase control, J. Biol. Chem. 276 (2001) 9670–9678.
[9] J. Gustavsson, S. Parpal, M. Karlsson, C. Ramsing, H. Thorn, M. Borg, M. Lindroth, K.H. Peterson, K.-E. Magnusson, P. Straylfors, Localization of the insulin receptor in caveolae of adipocyte plasma membrane, FASEB J. 13 (1999) 1961–1971.
[10] A. Kimura, S. Mora, S. Shigematsu, J.E. Pessin, A.R. Saltiel, The insulin receptor catalyzes the tyrosine phosphorylation of Caveolin-1, J. Biol. Chem. 277 (2002) 30153–30158.
[11] J. Inokuchi, Membrane microdomains and insulin resistance, FEBS Lett. 584 (2010) 1864–1871.
[12] S. Vainio, S. Heino, J.-E. Mansson, P. Fredman, E. Kuismanen, O. Vaarala, E. Ikonen, Dynamic association of human insulin receptor with lipid rafts in cells lacking caveolae, EMBO Rep. 31 (2002) 95–100.
[13] J. Sánchez-Wandelmer, A. Dávalos, E. Herrera, M. Giera, S. Cano, G. de la Peña, M.A. Lasunción, R. Busto, Inhibition of cholesterol biosynthesis disrupts lipid raft/caveolae and affects insulin receptor activation in 3T3-L1 preadipocytes, Biochim. Biophys. Acta, Biomembr. 1788 (2009) 1731–1739.
[14] T.T. Chiu, N. Patel, A.E. Shaw, J.R. Bamburg, A. Klip, Arp2/3- and cofilin-coordinated actin dynamics is required for insulin-mediated GLUT4 translocation to the surface of muscle cells, Mol. Biol. Cell (2010) (E10-04-0316).
[15] M. Foti, G.v. Porcheron, M. Fournier, C. Maeder, J.-L. Carpentier, The neck of caveolae is a distinct plasma membrane subdomain that concentrates insulin receptors in 3T3-L1 adipocytes, Proc. Natl. Acad. Sci. 104 (2007) 1242–1247.
[16] N. Andrews, K. Lidke, J. Pfeiffer, A. Burns, B. Wilson, J. Oliver, D. Lidke, Actin restricts FcεRI diffusion and facilitates antigen-induced receptor immobilization, Nat. Cell Biol. 10 (2008) 955–963.
[17] N.L. Andrews, J.R. Pfeiffer, A.M. Martinez, D.M. Haaland, R.W. Davis, T. Kawakami, J.M. Oliver, B.S. Wilson, D.S. Lidke, Small, mobile FcεRI receptor aggregates are signaling competent, Immunity 31 (2009) 469–479.
[18] B.G. Barisas, S. Smith, J. Liu, J. Song, G. Hagen, I. Pecht, D. Roess, Compartmentalization of the Type I Fc epsilon receptor and MAFA on 2H3 cell membranes, Biophys. Chem. 126 (2006) 209–217.
[19] D.S. Lidke, P. Nagy, R. Heintzmann, D. Arndt-Jovin, J. Post, H. Grecco, E. Jares-Erijman, T. Jovin, Quantum dot ligands provide new insights into erbB/HER receptor-mediated signal transduction, Nat. Biotechnol. 22 (2004) 198–203.
[20] K. Murase, T. Fujiwara, Y. Umemura, K. Suzuki, R. Iino, H. Yamashita, M. Saito, H. Murakoshi, K. Ritchie, A. Kusumi, Ultrafine membrane compartments for molecular diffusion as revealed by single molecule techniques, Biophys. J. 86 (2004) 4075–4093.
[21] Y. Sako, A. Kusumi, Compartmentalized structure of the plasma membrane for receptor movements as revealed by a nanometer-level motion analysis, J. Cell Biol. 125 (1994) 1251–1264.
[22] F. Daumas, N. Destainville, C. Millot, A. Lopez, D. Dean, L. Salomé, Confined diffusion without fences of a G protein coupled receptor as revealed by single particle tracking, Biophys. J. 84 (2003) 356–366.
[23] Y. Chen, J. Muller, P. So, E. Gratton, The photon counting histogram in fluorescence fluctuation spectroscopy, Biophys. J. 77 (1999) 553–567.
[24] T. Perroud, B. Huang, M.I. Wallace, R. Zare, Photon counting histogram for one-photon excitation, Chemphyschem 4 (2003) 1121–1123.
[25] D. Lidke, P. Nagy, B. Barisas, R. Heintzmann, J. Post, K. Lidke, A. Clayton, D. Arndt-Jovin, T. Jovin, Imaging molecular interactions in cells by dynamic and static fluorescence anisotropy (rFLIM and emFRET), Biochem. Soc. Trans. 31 (2003) 1020–1027.
[26] E. Jares-Erijman, T. Jovin, FRET imaging, Nat. Biotechnol. 21 (2003) 1387–1395.
[27] L.W. Runnels, S.F. Scarlata, Theory and application of fluorescence homotransfer to melittin oligomerization, Biophys. J. 69 (1995) 1569–1583.
[28] G.H. Patterson, D.W. Piston, B.G. Barisas, Förster distances between green fluorescent protein pairs, Anal. Biochem. 284 (2000) 438–440.
[29] K. Fogarty, J. McPhee, E. Scott, A. Van Orden, Probing the ionic atmosphere of single-stranded DNA using continuous flow capillary electrophoresis and fluorescence correlation spectroscopy, Anal. Chem. 81 (2009) 465–472.
[30] J. Ries, P. Schwille, New concepts for fluorescence correlation spectroscopy on membranes, Phys. Chem. Chem. Phys. 10 (2008) 3487–3497.
[31] S. Chiantia, J. Ries, P. Schwille, Fluorescence correlation spectroscopy in membrane structure elucidation, Biochim. Biophys. Acta 1788 (2009) 225–233.
[32] J. Jung, V.O. A, A three-state mechanism for DNA hairpin folding characterized by multiparameter fluorescence fluctuation spectroscopy, J. Am. Chem. Soc. 128 (2006) 1240–1249.
[33] J. Jung, R. Ihly, E. Scott, M. Yu, A. Van Orden, Probing the complete folding trajectory of a DNA hairpin using dual beam fluorescence correlation spectroscopy, J. Phys. Chem. B 112 (2008) 127–133.
[34] M.J. Saxton, Single-particle tracking: the distribution of diffusion coefficients, Biophys. J. 72 (1997) 1744–1753.
[35] A.N. Bader, S. Hoetzl, E.G. Hofman, J. Voortman, P.M.P. van Bergen en Henegouwen, G. van Meer, H.C. Gerritsen, Homo-FRET imaging as a tool to quantify protein and lipid clustering, Chemphyschem 12 (2011) 475–483.
[36] R. Varma, S. Mayor, GPI-anchored proteins are organized in submicron domains at the cell surface, Nature 394 (1998) 798–801.
[37] M. Rao, S. Mayor, Use of Forster's resonance energy transfer microscopy to study lipid rafts, Biochim. Biophys. Acta 1746 (2005) 221–233.

[38] S. Saffarian, U. Li, E. Elson, L. Pike, Oligomerization of the EGF receptor investigated by life cell fluorescence intensity distribution analysis, Biophys. J. 93 (2007) 1021–1031.
[39] Y. Chen, L.-N. Wei, J.D. Mauller, Probing protein oligomerization in living cells with fluorescence fluctuation spectroscopy, Proc. Natl. Acad. Sci. U. S. A. 100 (2003) 15492–15497.
[40] Y. Chen, L.-N. Wei, J.D. Müller, Unraveling protein-protein interactions in living cells with fluorescence fluctuation brightness analysis, Biophys. J. 88 (2005) 4366–4377.
[41] A.G. Godin, S. Costantino, L.-E. Lorenzo, J.L. Swift, M. Sergeev, A. Ribeiro-da-Silva, Y. De Koninck, P.W. Wiseman, Revealing protein oligomerization and densities in situ using spatial intensity distribution analysis, Proc. Natl. Acad. Sci. 108 (2011) 7010–7015.
[42] K.A.K. Tanaka, K.G.N. Suzuki, Y.M. Shirai, S.T. Shibutani, M.S.H. Miyahara, H. Tsuboi, M. Yahara, A. Yoshimura, S. Mayor, T.K. Fujiwara, A. Kusumi, Membrane molecules mobile even after chemical fixation, Nat. Methods 7 (2010) 865–866.
[43] A. Kusumi, Y.M. Shirai, I. Koyama-Honda, K.G.N. Suzuki, T.K. Fujiwara, Hierarchical organization of the plasma membrane: investigations by single-molecule tracking vs. fluorescence correlation spectroscopy, FEBS Lett. Front. Membr. Biochem. 584 (2010) 1814–1823.
[44] L.J. Pike, Rafts defined: a report on the Keystone symposium on lipid rafts and cell function, J. Lipid Res. 47 (2006) 1597–1598.
[45] E. Sheets, D. Holowka, B. Baird, Membrane organization in immunoglobulin E receptor signaling, Curr. Opin. Chem. Biol. 3 (1999) 95–99.
[46] R.D. Huby, R.J. Dearman, I. Kimber, Intracellular phosphotyrosine induction by major histocompatibility complex class II requires co-aggregation with membrane rafts, J. Biol. Chem. 274 (1999) 22591–22596.
[47] P. Oh, J.E. Schnitzer, Segregation of heterotrimeric G proteins in cell surface microdomains, Mol. Biol. Cell 12 (2001) 685–698.
[48] C.L. Manahan, M. Patnana, K.J. Blumer, M.E. Linder, Dual lipid modification motifs in Ga and Gg subunits are required for full activity of the pheromone response pathway in *Saccharomyces cerevisiae*, Mol. Biol. Cell 11 (2000) 957–968.
[49] A. Viola, R.L. Contento, B. Molon, in: T. Saito, F.D. Batista (Eds.), Immunological Synapse, vol. 340, Springer Berlin Heidelberg, 2010, pp. 109–122.
[50] C. Dietrich, B. Yang, T. Fujiwara, A. Kusumi, K. Jacobson, Relationship of lipid rafts to transient confinement zones detected by single particle tracking, Biophys. J. 82 (2002) 274–284.
[51] K. Ritchie, R. Iino, T. Fujiwara, K. Murase, A. Kusumi, The fence and picket structure of the plasma membrane of live cells as revealed by single molecule techniques, Mol. Membr. Biol. 20 (2003) 13–18.